Microsc. Microanal. 20, 671–677, 2014
doi:10.1017/S1431927614000129

Microscopy AND Microanalysis

Is Localized Infrared Spectroscopy Now Possible in the Electron Microscope?

Peter Rez*

Department of Physics, Arizona State University, Tempe, AZ 82287-1504, USA

Abstract: The recently developed in-column monochromators make it possible to record energy-c spectra with resolutions better than 30 meV from nanometer-sized regions. It should therefore in principle be possible to detect localized vibrational excitations. The scattering geometry in the electron microscope means that bond stretching in the specimen plane or longitudinal optic phonons dominate the scattering. Most promising for initial studies are vibrations with energies between 300 and 400 meV from hydrogen bonded to other atoms. Estimates of the scattering cross-sections on the basis of a simple model show that they are about the same as inner shell scattering cross-sections. Cross-sections also increase with charge transfer between the atoms, and theory incorporating realistic charge distributions shows that signal/noise is the only limitation to high-resolution imaging. Given the magnitude of the scattering cross-sections, minimizing the tail of the zero-loss peak is just as important as achieving a small-width at half-maximum. Improvements in both resolution and controlling the zero-loss tail will be necessary before it is practical to detect optic phonons in solids between 40 and 60 meV.

Key words: energy loss, infrared, Raman, optic phonon, cross-section

Introduction

The development of the new generation of monochromators has made it possible to record energy-loss spectra with an energy resolution of 30 meV from regions <1 nm across (Krivanek et al., 2013a). This is almost an order of magnitude improvement over what was possible with monochromators in the electron gun (Mook & Kruit, 1999). Substituting improved power supplies for the spectrometer could potentially give energy resolutions of 10 meV (Krivanek et al., 2013b). Lines from absorption due to bond stretching in molecules, especially for hydrogen atoms bound to other atoms, are between 300 and 400 meV. Optic phonons in solids such as semiconductors have energies in the range 40–60 meV. In principle, these spectral features, that have hitherto been the province of infrared (IR) and Raman spectroscopy, are now observable by electron energy-loss spectroscopy (EELS). Whether they will be detected in practice depends on the scattering cross-section and its magnitude in relation to the background from the tail of the zero-loss peak.

The earlier work on the effects of phonon scattering in electron microscopy have concentrated on acoustic phonons and their effects on diffraction contrast, in particular, anomalous absorption (Hashimoto et al., 1962; Rez, 1983). Later work was inspired by the need for a quantitative theory for high-angle annular dark-field imaging (Amali & Rez, 1997) and as an explanation for the "Stobbs" effect in high-resolution phase contrast images (Hytch & Stobbs, 1994; Herring, 2006). The earlier theories can be generalized to address scattering by optic phonons or molecular vibrations. To estimate the magnitude and angular dependence of the scattering cross-section, a simplified model that either describes the stretching of a single bond, or the optical vibration of a linear chain with two distinct atoms, has been used. The linear chain with two distinct atoms clearly demonstrates the significant difference between acoustic and optical phonons (Kittel, 1986). For acoustic modes the two atoms move in phase, for optical modes they vibrate in antiphase. If one of the atoms has a positive charge and the other an equal negative charge then the oscillation gives a time varying dipole that will either absorb or emit electromagnetic radiation (see Fig. 1).

Geometrical considerations alone suggest that scattering from longitudinal vibrations or bond stretches in the plane of the specimen will dominate any measured spectrum. The scattering cross-sections for optical vibrations are quite large, comparable to the cross-section for a 10 eV window at the Carbon K edge for typical collection angles. Light atoms such as hydrogen have large displacements that lead to large cross-sections, as do charge transfers. Calculations indicate that with the measured background from the zero-loss tail it might be possible to detect a single C–H bond, so making hydrogen mapping a distinct possibility. The larger measured zero-loss tail at 50 meV precludes detection of optic phonons in semiconductors, though this might become possible if the zero loss were sharpened to have a full-width at half-maximum of 10 meV. Finally, the form of the angular distribution suggests that atomic resolution in these modes will be possible, provide there is sufficient signal and that the resolution is not totally determined by signal/noise considerations.

Received September 9, 2013; accepted December 31, 2014
*Corresponding author. Peter.Rez@asu.edu

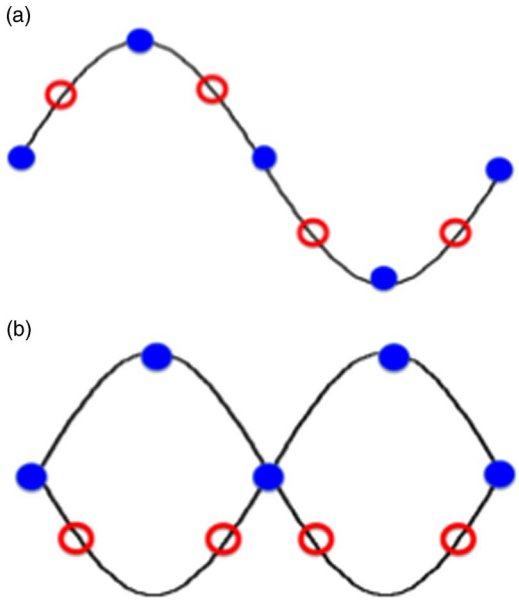

Figure 1. Vibrations of a linear chain with two types of atoms (shown as filled and open circles). The upper figure (**a**) shows an acoustic mode where all the atoms vibrate in phase, the lower figure (**b**) shows an optic mode where the two atom types vibrate in antiphase. If one atom is positively charged and the other negatively charged this clearly gives rise to an oscillating dipole.

Theory

The vibrations of atoms in a solid or a molecule are best described as small oscillations governed by classical equations of motion (Born, 1954):

$$m_i \frac{d^2 u_i}{dt^2} = -K_{ij} u_j, \tag{1}$$

where m_i is the mass of atom i, u_i is its displacement and K_{ij} is the matrix of elastic constants known as the Hessian matrix. It can be calculated by taking the second derivative with respect to displacement of the total energy, E:

$$K_{ij} = \frac{d^2 E}{du_i du_j}. \tag{2}$$

In a solid the displacements are Bloch functions and the index i refers to an atom position $\mathbf{r}_i$ within the primitive unit cell:

$$\mathbf{u}(\mathbf{r_i}, t) = \mathbf{u_i}(\mathbf{q}) \exp(i\mathbf{q}.\mathbf{r}_i - i\omega(q)t), \tag{3}$$

where $\mathbf{q}$ is the wavevector of the excitation and ω is the frequency which is a function of $\mathbf{q}$ as are the relative amplitudes $\mathbf{u_i}$ for the different atoms. In a molecule there is no dispersion and the displacements are

$$\mathbf{u}(\mathbf{r_i}, t) = \mathbf{u_i} \exp(-i\omega t). \tag{4}$$

The isolated molecule might be more relevant than the continuous perfect solid as it more closely resembles the defects that will be studied by atomic-resolution spectroscopy.

For convenience, in a molecule or a solid with many atoms in the primitive cell, it is more convenient to use a vector notation and rewrite equation (1) as

$$\mathbf{m} \frac{d^2 \mathbf{u}}{dt^2} = -\mathbf{K}\mathbf{u}, \tag{5}$$

where $\mathbf{m}$ is a vector representing the masses of the different atoms and $\mathbf{K}$ is the Hessian matrix. A simple transformation to mass weighted displacements $\mathbf{v}$ makes it possible to write a solution in terms of the normal modes or eigenfrequencies,

$$\begin{aligned} \mathbf{v} &= \mathbf{m}^{\frac{1}{2}}\mathbf{u} \\ \mathbf{u} &= \mathbf{m}^{-\frac{1}{2}}\mathbf{v}, \end{aligned} \tag{6}$$

$$\begin{aligned} \mathbf{H} &= \mathbf{C}\omega^2\mathbf{C}^{-1} \\ \mathbf{v} &= \mathbf{C}\exp(i\omega t) \\ \mathbf{u} &= \mathbf{m}^{-\frac{1}{2}}\mathbf{C}\exp(i\omega t). \end{aligned} \tag{7}$$

The first stage in calculating the scattering cross-section is to consider the effect on the potential seen by the fast electron $V(\mathbf{r})$. For generality we will start with a crystal whose potential is given by

$$\begin{aligned} V(\mathbf{r}) &= \sum_{l,n} V_n(\mathbf{r} - (\mathbf{r}_n + \mathbf{r}_l + \mathbf{u}_n)) \\ V(\mathbf{r}) &= \frac{V_c}{(2\pi)^3} \int \sum_{l,n} v_n(\mathbf{q}) \exp(i\mathbf{q}.\mathbf{r} - \mathbf{q}.(\mathbf{r}_n + \mathbf{r}_1 + \mathbf{u}_n)) d^3q \\ \Delta V(\mathbf{r}) &= \frac{V_c}{(2\pi)^3} \int \sum_{l,n} -i\mathbf{q}.\mathbf{u}_n v_n(\mathbf{q}) \exp(i\mathbf{q}.\mathbf{r} - \mathbf{q}.(\mathbf{r}_n + \mathbf{r}_1)) d^3q, \end{aligned} \tag{8}$$

where n labels the atom, l the lattice site, $\mathbf{u}_n$ the displacement, and V_c the volume of the unit cell. The potential contribution from a single atom can also be expressed in terms of the electron scattering factor (Rez, 2001):

$$f_n^{el}(q) = \frac{2me}{\hbar^2} v_n(q). \tag{9}$$

The displacement is small and so the part of the exponential with the displacement can be expanded to first order. At this point we should introduce fast electron states where the superscript i denotes the initial states, f denotes the final or scattered states, z is a depth in the specimen, and $\mathbf{g}$ and $\mathbf{h}$ are reciprocal lattice vectors:

$$\begin{aligned} \psi_i(\mathbf{r}) &= \sum_g \phi_g^i \exp(i(\mathbf{k}_i + \mathbf{g}).\mathbf{r}) \\ \psi_f(\mathbf{r}) &= \sum_h \phi_h^f \exp\left(i\left(\mathbf{k}_f + \mathbf{h}\right).\mathbf{r}\right). \end{aligned} \tag{10}$$

The amplitudes at depth z can be found by any of the standard techniques such as matrix diagonalization to give Bloch wave eigenvectors or they can be the solutions from the multislice algorithm. Integrating over the fast electron coordinate $\mathbf{r}$ and summing over the unit cells gives conversation of momentum:

$$\mathbf{q} = \mathbf{k}_f - \mathbf{k}_i + \mathbf{g} - \mathbf{h}. \tag{11}$$

Wavevectors where $g-h\neq 0$ correspond to Umklapp scattering. The displacements can be expressed in terms of phonon creation and destruction operators. Since optic phonon energies are greater than k_BT it is unlikely that these phonons or vibrations are present at room temperature and so only the creation term applies.

The total differential cross-section in the general case is

$$\frac{dI}{d\Omega}=\frac{1}{V_c}\sum\left|\phi_h^{f^*}(z)(\mathbf{k}_f-\mathbf{k}_i+\mathbf{g}-\mathbf{h})\mathbf{m}^{-\frac{1}{2}}\mathbf{C}^{*T}\mathrm{f}_{el}(\mathbf{k}_f-\mathbf{k}_i+\mathbf{g}-\mathbf{h})\right.$$
$$\left.\times\left(\frac{\hbar N_0\left(\omega\left(k_j-k_i+g-h\right)+1\right)}{2\omega\left(k_f-k_i+g-h\right)}\right)^{\frac{1}{2}}\phi_g^i(z)\right|\Delta z, \qquad (12)$$

where $N_0(\omega)$ is the Bose Einstein factor.

Approximations

The essential features of vibrational, or optic phonon, scattering can be understood on the basis of a considerably simplified model. Since we are only interested in calculating cross-sections, not the details of image contrast, the fast electron states will be represented as plane waves. As a further simplification only a stretch vibration in a diatomic molecule will be considered. There is only one vibrational frequency given by

$$\omega=\left(2K\frac{(m_1+m_2)}{m_1m_2}\right)^{\frac{1}{2}}, \qquad (13)$$

where m_1 and m_2 are the masses of the two atoms.

There is no longer a variation of frequency or excitation amplitude with wavevector. Equation (12) simplifies to

$$\frac{d\sigma}{d\Omega}=\left|\mathbf{q}.\mathbf{e}\left(\frac{\hbar(N_0(\omega)+1)}{2\omega}\right)^{\frac{1}{2}}\left(\sqrt{\frac{m_2}{m_1}}\frac{f_{el;1}(q)}{\sqrt{m_1+m_2}}-\sqrt{\frac{m_1}{m_2}}\frac{f_{el;2}(q)}{\sqrt{m_1+m_2}}\right)\right|^2. \qquad (14)$$

This equation will be used to estimate the magnitude of the scattering cross-section. To investigate the effects of charge transfer the Mott expression is used for the electron scattering factor (Mott & Massey, 1965):

$$f_{el}(q)=\frac{2}{a_0}\frac{(Z-f_x(q))}{q^2}, \qquad (15)$$

where Z is the atomic number, $f_x(q)$ is the X-ray scattering factor, and a_0 the Bohr radius.

As a further simplification it will be assumed that any ionic charge is concentrated at the nucleus. This approximation is equivalent to using partial charges to calculate IR absorption in chemistry or biophysics. Neglecting any other electron rearrangements due to ionicity, the electron scattering factor can now be written as

$$f_{el}^{\text{ion}}(q)=\frac{2\Delta Q}{a_0q^2}+f_{el}^{\text{neut}}(q), \qquad (16)$$

where ΔQ is the charge transfer between the two atoms. From equation (14) it can be seen that the differential cross-section is proportional to the difference between the electron scattering factor for each atom, divided by its atomic mass. Since both electron scattering factors and atomic masses are approximately proportional to atomic number this difference will be small and can be neglected.

The differential cross-section is now proportional to ΔQ^2 and is approximately given by

$$\frac{d\sigma}{d\Omega}=\frac{4}{a_0^2}\left|\frac{2\mathbf{q}.\mathbf{e}\Delta Q}{q^2}\left(\frac{\hbar(N_0(\omega)+1)}{2\omega}\right)^{\frac{1}{2}}\sqrt{\frac{(m_1+m_2)}{m_1m_2}}\right|^2 \qquad (17)$$

Results

The scattering geometry is defined by equations (8) and (14) or (17). Just as in EELS the wavevector **q** has components both parallel to the incident beam, q_z, which for convenience we will assume is normal to the specimen surface, and perpendicular to the incident beam, q_x and q_y. The parallel component is

$$q_z=K\frac{\Delta E}{mv^2}, \qquad (18)$$

where K is the fast electron wavevector and v is the velocity of the fast electron. This is normally expressed as a characteristic angle θ_E. Since the energy losses, ranging from 50 to 400 meV, are so small the angles are microradians, very small compared to typical collection angles of tens of milliradians used in electron microscopy! The wavevector therefore lies in the specimen plane. Equation (8) has a scalar product between a displacement or polarization vector and the wavevector. To maximize the scattering the displacement has to be in the same direction as the scattering wavevector, in the plane of the specimen. Therefore, the strongest contribution comes from longitudinal optic phonons, as shown in Figure 2. For molecular vibrations, which have no dispersion and do not depend on wavevector, the displacements still have to be in the plane of the specimen though they could be either torsional vibrations with displacements perpendicular to a bond or simple bond stretching motions.

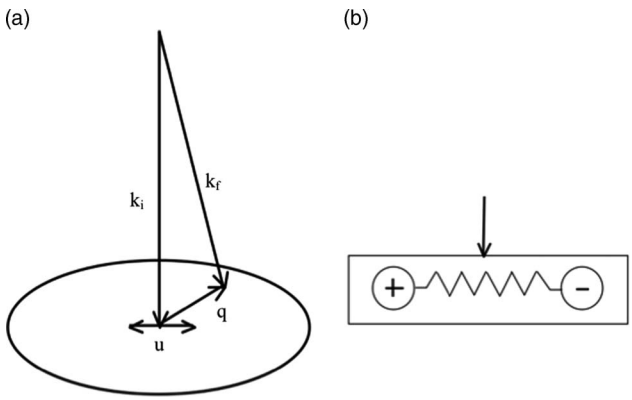

Figure 2. Scattering geometry for optic phonon or vibrational scattering. **a**: The incident wavevector of the fast electron is represented by $\mathbf{k_i}$, the wavevector of the scattered fast electron by $\mathbf{k_f}$. The scattering wavevector **q**, is in the plane of the specimen, as are the atomic displacements **u**. **b**: The fast electron is shown incident normal to the "bond" between the positively and negatively charged ions, represented as a spring, and the specimen surface.

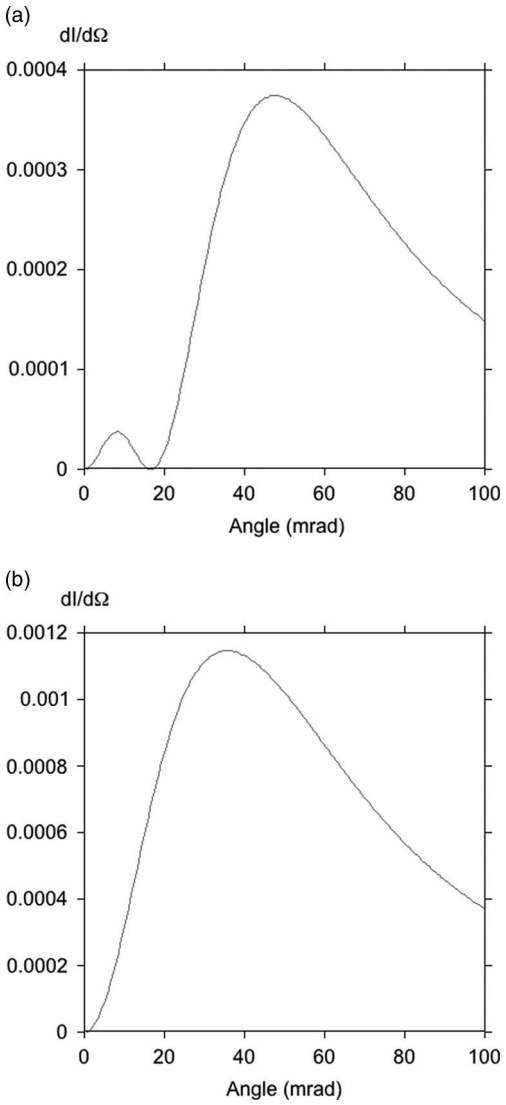

Figure 3. Differential cross-section for scattering of 100 keV electrons from (**a**) a C–H bond stretch and (**b**) Fe–H bond stretch.

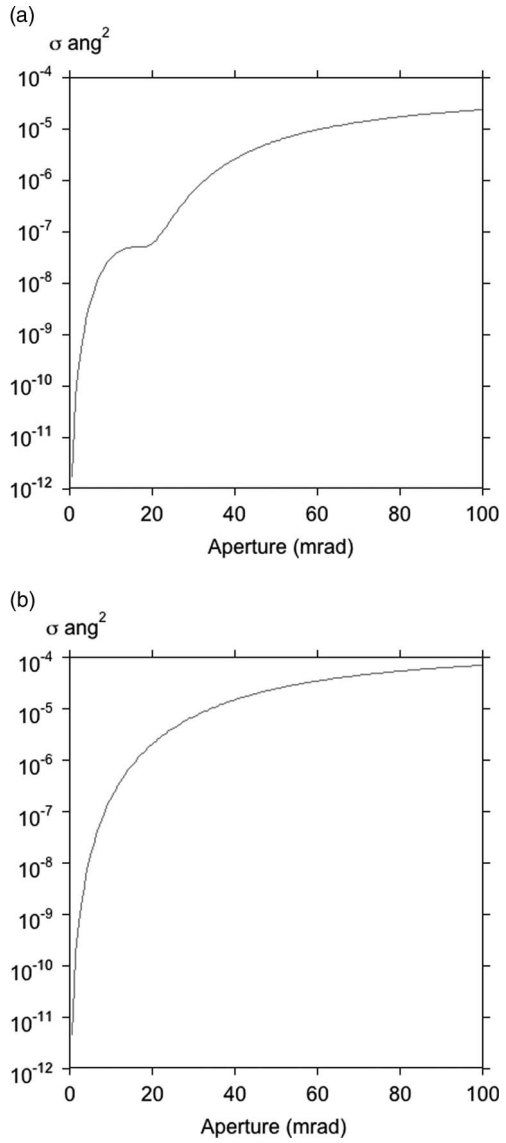

Figure 4. Integrated scattering cross-section for scattering from (**a**) C–H (**b**) Fe–H.

From the theory it can be clearly seen that the displacements of light elements are larger, leading to a higher cross-section. IR spectroscopy shows that stretching modes of hydrogen strongly bound to other atoms have the highest frequencies, normally in the range of 2,500–3,500 cm^{-1} corresponding to 300–400 meV. Given the clear separation between these spectral features and the zero-loss peak they should be easily accessible using monochromated EELS. The angular dependence can be calculated from equation (14) and is shown for a C–H and a Fe–H stretch in Figure 3 for 100 keV electrons. The vibration frequencies are taken from tabulations of IR frequencies (Lambert et al., 1998; Andrews, 2004).

Just as with acoustic phonons the product of $q^2 f_{el}^2(q)$ shifts the maximum to larger angles, in this case about 40 mrad. The zero in the differential cross-section is a real effect, the two electron scattering factors have slightly different variation with scattering angle, but at one point the lighter element scattering factor multiplied by the ratio of masses $\frac{m_2}{m_1}$, where m_2 is the heavier mass, is identical to the heavier atom scattering factor and the term inside the brackets is zero. The integrated cross-sections are shown in Figure 4.

Nearly all the scattering is collected with a 60 mrad aperture, and a large part of the scattering is collected with a 40 mrad aperture that nicely matches the beam convergence in the fifth order aberration-corrected Nion UltraSTEM, Kirkland, WA.

Charge transfer increases the total cross-section since it increases the magnitude of the oscillator dipole, as is apparent from equation (17). The cross-section can also be written in terms of $\mathrm{Im}\left(\frac{1}{\varepsilon(\Delta E,q)}\right)$ where $\varepsilon(\Delta E, q)$ is the energy and wavevector-dependent dielectric function. Plots of the variation of $\mathrm{Im}\left(\frac{1}{\varepsilon(\Delta E,0)}\right)$ in the IR region derived from the optical data compilation of Palik (1985) is given in Figure 5. Note the difference by almost six orders of magnitude

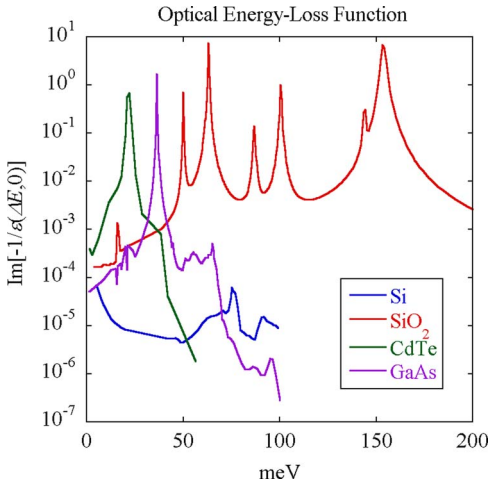

Figure 5. Optical energy-loss function in the infrared region.

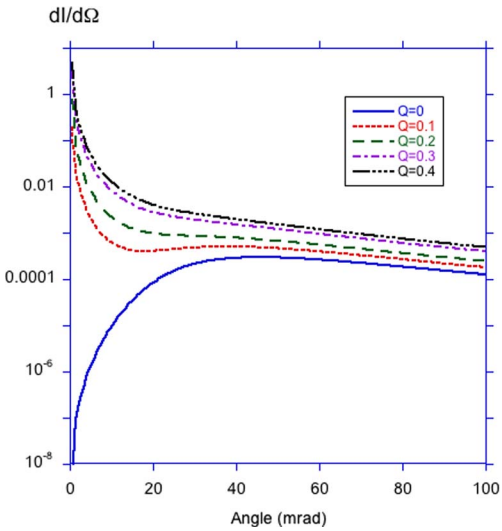

Figure 6. Differential cross-section for scattering of 100 keV electrons by stretching of an O–H bond for different values of charge transfer ΔQ, calculated from equation (17).

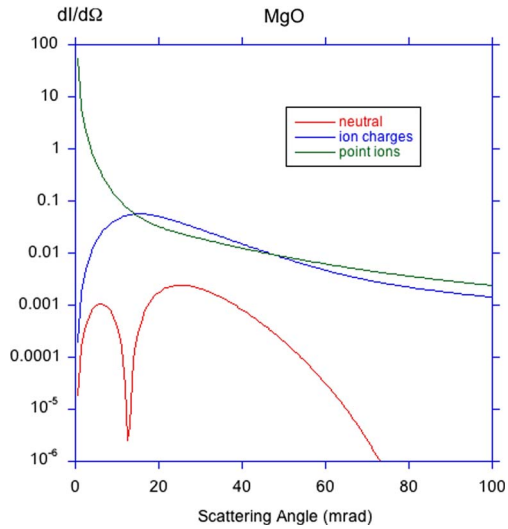

Figure 7. Differential scattering cross-section for scattering of 100 keV electrons by MgO stretching vibration with different assumptions for ionicity.

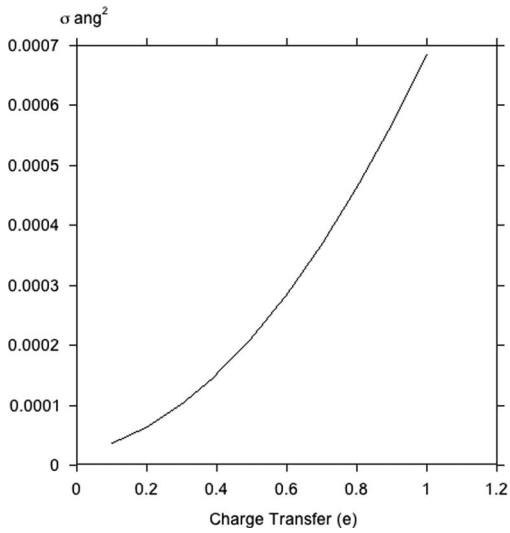

Figure 8. Differential cross-section for scattering from an OH atom pair by 100 keV electrons.

between silicon that has two atoms in the primitive unit cell with equal charge, and silica where there is considerable charge transfer.

The O–H bond in some organics would be a good candidate for an atom pair where there is potential for charge transfer. Figure 6 shows the angular distribution, calculated using equation (17).

According to this model, which is the same as that used by Geiger & Wittmack (1965) in their calculations of IR scattering from small molecules, the charge transfer leads to a large peak for very small scattering angles. One would therefore expect that the scattering would be very delocalized, and that high-resolution imaging using these optical vibrations would be impossible (Egerton, 2013), contrary to the case with acoustic modes (Rez, 1993). The peak is an artifact of the simple theory that assigns point charges (in molecular dynamics studies these would be called partial charges) at the nuclear positions. Rez et al., (1994) have published tables of scattering factors for ions as well as neutral atoms. For a highly ionic material such as MgO the ionic charge density is a very good approximation to the actual measured charge density or the charge density calculated from first principles density functional theory. In Figure 7 it can be seen that the differential cross-section for ionic scattering factors is similar to that from the neutral atoms, though considerably larger in magnitude. It does not show a peak for small scattering angles. The neutral atom differential cross-section goes to zero at 15 mrad for the same reasons as discussed above for the C–H stretch differential cross-section. It would therefore appear that all differential

Table 1. Integrated Scattering Cross-Sections for Scattering of 100 keV Electrons from Stretching Vibrations in Different Atom Pairs.

	Energy (meV)	Energy (cm^{-1})	σ ($Å^2$)
C–H	375	3,000	2.39×10^{-5}
O–H	460	3,700	1.98×10^{-5}
Ni–H	265	2,119	5.12×10^{-5}
Fe–H	212	1,694	7.04×10^{-5}
Zr–H	200	1,608	8.38×10^{-5}
W–H	240	1,922	8.25×10^{-5}
GaAs	50	~400	9.12×10^{-5}
CdTe	50	~400	1.42×10^{-5}
MgO	63	~500	2.87×10^{-5}
MgO (ion)	63	~500	8.35×10^{-4}

Table 2. Cross-Sections Integrated Over Different Energy Windows from Threshold for Ionization of the Carbon K Edge by 100 keV Electrons.

	10 mrad, σ ($Å^2$)	100 mrad, σ ($Å^2$)
1 eV	7.1×10^{-7}	1.0×10^{-6}
10 eV	6.5×10^{-6}	8.8×10^{-6}
40 eV	2.1×10^{-5}	3.3×10^{-5}

cross-sections have maxima at angles between 20 and 40 mrad, which would suggest that atomic-resolution imaging should be possible, if it is not limited by signal/noise considerations. The total cross-section for O–H stretching as a function of charge transfer calculated from equation (17) is shown in Figure 8. Not surprisingly on this simple model it increases as the square of the charge transfer.

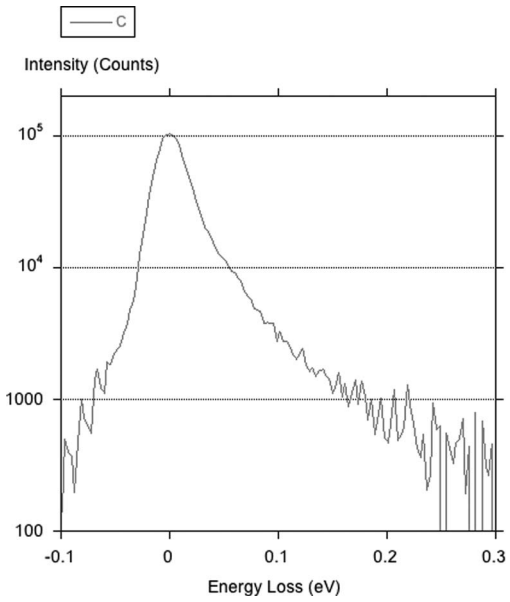

Figure 9. Zero-loss peak, 30 meV full-width at half-maximum.

It is instructive to compare integrated cross-sections for various hydrides or hydrogen bonded to other atoms and estimated cross-sections for optic phonons. The results are as Table 1. The cross-section is greater for some of the heavy element hydrides, though this is mainly due to the weaker bond resulting in a lower vibrational frequency. Equation (14) shows that the cross-section is inversely proportional to the frequency, just as with acoustic phonons (Table 2)

These scattering cross-sections are quite large, for comparison, the differential cross-sections integrated over different windows at the C K edge are shown for 10 and 100 mrad (Egerton, 1979). The optical vibration cross-section is comparable to the C K cross-section for a 40 eV window. It would therefore seem that detection of the vibration attributable to a single atom, for example, a single H atom at an interstitial site or a single OH bond, is well within the bounds of practicality. Whether it can actually be done in practice will depend on the background in the band gap region from the zero-loss tail, not to mention multiple scattering from other IR or optical phonon losses.

Figure 9 shows a logarithmic plot of the zero-loss peak. The intensity is about 5% of the maximum at 50 meV, typical of the energies of optic modes in semiconductors, but only 10^{-3}–10^{-4} of the zero-loss maximum in the region between 300 and 500 meV. It should therefore be possible to detect a single H atom in an iron matrix or a single O–H bond assuming $1e^-$ charge transfer or five O–H bonds without charge transfer. It is conceivable that if the shape of the zero-loss peak does not change, lowering the full-width at half-maximum from 30 to 10 meV might make the semiconductor optic modes accessible.

Conclusions

Energy resolutions of 30 meV make it possible to observe features in the IR region of the electromagnetic spectrum. Geometrical considerations show that modes with displacements in the specimen such as longitudinal optic modes will dominate. Most promising are stretching of strong bonds involving H atoms that involve vibrational energies between 300 and 500 meV. The differential cross-section reaches a maximum at angles comparable to the beam convergence in aberration-corrected microscopes, so in principle high-resolution imaging will be possible. Cross-sections are quite large, comparable to those used for mapping well-known inner shell edges. In particular there are large cross-sections for vibrations involving light atoms such as H, and not surprisingly charge transfer leads to substantial increases in cross-section. In practice the detection of atomic vibrations will be limited by the tail of the zero-loss peak. In the absence of interference from multiple scattering it might be possible to detect the vibration of a single H atom in an Fe matrix or attached to an oxygen atom if there is substantial charge transfer. The detection of semiconductor optic modes will have to wait until resolution is improved to 10 meV or better.

Acknowledgments

I would like to thank Dr. O.L. Krivanek for making me investigate this problem, Prof R.F. Egerton for many discussions, Dr. R. Narayan for preparing Figure 5, Jing Tao Zhu for Figure 9.

References

Amali, A. & Rez, P. (1997). Theory of lattice resolution in high angle annular dark field images. *Microsc Microanal* **3**, 28–46.

Andrews, L. (2004). Matrix infrared spectra and density functional calculations of transition metal hydrides and dihydrogen complexes. *Chem Soc Rev* **33**, 123–132.

Born, M. (1954). *Dynamical Theory of Crystal Lattices*. Oxford: Clarendon Press.

Egerton, R.F. (1979). K-shell ionization cross-sections for use in microanalysis. *Ultramicroscopy* **4**, 169–179.

Egerton, R.F. (2013). Prospects for vibrational EELS with high spatial resolution. *Microsc Microanal*.

Geiger, J. & Wittmack, K. (1965). Wirkungsquerschnitte fur die Anregung von Molekulschwingungen durch schnelle Elektronen. *Z Physik* **187**, 433–443.

Hashimoto, H., Howie, A. & Whelan, M.J. (1962). Anomalous electron absorption effects in metal foils: Theory and comparison with experiment. *Proc Roy Soc* **A269**, 80–103.

Herring, R.A. (2006). Coherence measurements of zero-loss, plasmon-loss and phonon-loss electrons and their contribution to the Stobbs factor. *Ultramicroscopy* **106**, 960–961.

Hytch, M.J. & Stobbs, W.M. (1994). Quantitative comparison of high resolution TEM images with image simulations. *Ultramicroscopy* **53**, 191–203.

Kittel, C. (1986). *Introduction to Solid State Physics*. New York: Wiley.

Krivanek, O.L., Lovejoy, T.C., Delby, N. & Carpenter, R.W. (2013a). Monochromated STEM with a 30 meV-wide, atom-sized electron probe. *Microscopy* **62**(1), 3–21.

Krivanek, O.L., Lovejoy, T.C., Murfitt, M.F., Skone, G., Batson, P.E., Delby, N., Rez, D., Rez, P. & Grant, I.P. (2013b). Advances in monochromated STEM and EELS, EMAG. York, I.O.P.

Lambert, J.B. & Shurvell, H.F. et al. (1998). *Organic Structural Spectroscopy*. Upper Saddle River: Prentice Hall.

Mook, H.W. & Kruit, P. (1999). On the monochromatisation of high brightness electron sources for electron microscopy. *Ultramicroscopy* **78**, 43–51.

Mott, N.F. & Massey, H.S.W. (1965). *The Theory of Atomic Collisions*. Oxford: Clarendon Press.

Palik, E.D. (1985). *Handbook of Optical Constants of Solids*. Orlando: Academic Press.

Rez, D., Rez, P. et al. (1994). Dirac-Fock calculations of X-ray scattering factors and contributions to the mean inner potential for electron scattering. *Acta Cryst A* **50**, 481–497.

Rez, P. (1983). The contrast of defects in inelastically scattered electrons. *Acta Cryst A* **39**, 697–706.

Rez, P. (1993). Does phonon scattering give high resolution images? *Ultramicroscopy* **52**, 260–266.

Rez, P. (2001). Scattering cross sections in electron microscopy and analysis. *Microsc Microanal* **7**, 356–362.